

D-galactose receptor-targeted *in vivo* spectral fluorescence imaging of peritoneal metastasis using galactosamin-conjugated serum albumin-rhodamine green

Yukihiro Hama

National Institutes of Health
National Cancer Institute
Center for Cancer Research
Molecular Imaging Program
Bethesda, Maryland 20892-1088

Yasuteru Urano

The University of Tokyo
Graduate School of Pharmaceutical Sciences
7-3-1 Hongo
Bunkyo-ku, Tokyo 113-0033
Japan

Yoshinori Koyama

Peter L. Choyke

Hisataka Kobayashi

National Institutes of Health
National Cancer Institute
Center for Cancer Research
Molecular Imaging Program
Bethesda, Maryland 20892-1088

Abstract. The wavelength resolved spectral fluorescence imaging technique using a fluorescein-conjugated avidin has been reported to visualize submillimeter implants of ovarian cancer because of its highly targeted and quickly cleared pharmacokinetics. However, clinical application of avidin was hampered by its strong immunogenicity. As a clinically feasible alternative to avidin, which targets the same D-galactose receptor but is made from a nonimmunogenic source, with even better binding capability by multiplying binding sites but still maintaining a favorable characteristic of high isoelectric point, a serum albumin conjugated with 23 galactosamine and 2 rhodamine green molecules (GmSA-RhodG) was designed and synthesized. GmSA-RhodG showed more than 10-fold rapid and higher uptake by SHIN3 ovarian cancer cells than both avidin- and no galactosamine-conjugated albumin (bovine serum)-RhodG. Sensitivity and specificity of GmSA-RhodG to detect red fluorescence labeled peritoneal cancer foci in mouse cancer model were 100%/99% ($n=566$), respectively for ~ 1 -mm lesions and even smaller lesions were detected *in vivo*. These results indicate that GmSA-RhodG is not only a clinically feasible alternative but more efficient targeting reagent for D-galactose receptors than avidin-RhodG. © 2007 Society of Photo-Optical Instrumentation Engineers. [DOI: 10.1117/1.2779351]

Keywords: molecular imaging; ovarian cancer; clinical application; multivalency; *in vivo* spectral fluorescence imaging; D-galactose receptor.

Paper 06277SSR received Oct. 3, 2006; revised manuscript received Feb. 2, 2007; accepted for publication Feb. 5, 2007; published online Sep. 25, 2007.

1 Introduction

Image-guided endoscopic surgery has become a common procedure in the abdominal and thoracic cavities, because it is less invasive than open surgery.¹⁻³ It is recognized that such procedures may be improved by optically enhanced imaging using fluorescent probes. To improve their utility, fluorescence probes must be designed so as to yield a high target-to-background ratio that can be achieved in several ways. One approach is to utilize targeting ligands linked to fluorophores that bind to cancers, whereas unbound fluorophores are absorbed and removed from the field of view.

Prior reports have described a fluorescein-conjugated avidin (Av-FITC) and an avidin conjugated with rhodamine green (Av-RhodG), which were able to visualize submillimeter cancer implants in the peritoneal cavity with acceptable signal-to-background ratios.⁴ This conjugate relies on the affinity of avidin for lectin binding protein (synonyms of asialo receptors, β -D-galactose receptors) on the cell surface of

wide variety of cancers arising from the ovary, pancreas, colon, and stomach, which can spread in peritoneal space.⁵ Unbound avidin is rapidly removed from the peritoneal cavity by absorption and taken to the liver. Thus, high target-to-background ratios are achieved. However avidin, which is derived from a hen egg protein, is not clinically practical because of its well-known immunogenicity in humans.^{6,7} As a clinically feasible alternative to avidin, which can still target the cell surface D-galactose receptor but is made from non-immunogenic materials, with even better binding capability by multiplying binding sites but still maintaining a favorable characteristic of high isoelectric point, a serum albumin conjugated with 23 galactosamine and 2 rhodamine green molecules (GmSA-RhodG) was designed and synthesized by conjugation of D-galactosamines to carboxyl groups yet can be conjugated with rhodamine green (GmSA-RhodG) to amide groups on the albumin. The purpose of this study was to synthesize and evaluate GmSA-RhodG for its ability to bind ovarian cancer cells *in vitro* and compare the fluorescence intensity of bound GmSA-RhodG to bound Av-RhodG *in vivo* in a mouse model of ovarian cancer peritoneal metastases to de-

Address all correspondence to Hisataka Kobayashi, MD, PhD, NCI/NIH, Center for Cancer Research, Molecular Imaging Program, Bldg. 10, Rm 1B40, MSC 1088, 10 Center Dr., Bethesda, Maryland 20892-1088. Tel: 301-435-4086; Fax: 301-402-3191; E-mail: Kobayash@mail.nih.gov.

velop a clinically feasible method for the D-galactose receptor-targeted molecular cancer imaging.

2 Materials and Methods

2.1 Synthesis of Avidin-Conjugated Green Fluorescence Dyes

Avidin was purchased from Pierce Biochemical Inc. (Milwaukee, Wisconsin), bovine serum albumin (BSA) and galactosamine-conjugated bovine serum albumin (GmSA), which contained 23 galactosamine molecules on a single albumin molecule, were purchased from Sigma Chemical (St. Louis, Missouri), amido-reactive RhodG was purchased from Molecular Probes Inc. (Eugene, Oregon). At room temperature, 400 μg (5.9 nmol) of GmSA, BSA, and avidin in 196 μL of Na_2HPO_4 was incubated with 24 nmol (4 μL /6 mM) of RhodG-succinimidyl ester, respectively, in dimethyl sulfoxide (DMSO) for 15 min. The mixture was purified with Sephadex G50 (PD-10; GE Healthcare, Milwaukee, Wisconsin). GmSA-, BSA-, and avidin-conjugated RhodG samples (GmSA-RhodG, BSA-RhodG, and Av-RhodG, respectively) were kept at 4°C in the refrigerator as stock solutions.

The protein concentration of GmSA-RhodG, BSA-RhodG, and Av-RhodG samples was determined with Coomassie Plus protein assay kit (Pierce Chemical Company, Rockford, Illinois) by measuring the absorption at 595 nm with a visible ultraviolet (UV-vis) system (8453 Value UV-Bis system, Agilent Technologies, Palo Alto, California) using GmSA, BSA, and avidin standard solutions of known concentrations (100, 200, and 400 $\mu\text{g}/\text{mL}$). Then, the RhodG concentrations were measured by the absorption at 503 nm, respectively, with a UV-vis system to confirm the number of fluorophore molecules conjugated with each avidin, BSA, or GmSA molecule. By changing the concentration of the avidin, BSA, or GmSA solution, the number of fluorophore molecules per avidin, BSA, or GmSA was adjusted to be 2.0.

2.2 Cell Culture

An established ovarian cancer cell line SHIN3 Ref. 8 was used for *in vitro* fluorescence microscopy, flow cytometry, and *in vivo* optical imaging for intraperitoneal disseminated cancer implants. The cell lines were grown in RPMI 1640 medium (Gibco, Gaithersburg, Maryland) containing 10% fetal bovine serum (FBS) (Gibco), 0.03% L-glutamine at 37°C, 100 units/mL penicillin, and 100 $\mu\text{g}/\text{mL}$ streptomycin in 5% CO_2 .

2.3 Transfection of Red Fluorescence Protein (DsRed2) to the SHIN3 Cell

The red fluorescence protein (RFP DsRed2)-expressing plasmid was purchased from Clontech Laboratories Inc. (Mountain View, California). The plasmid was transfected into the SHIN3 cells to validate the results with the targeted fluorophores (*vide infra*). The transfection of RFP was performed with the electroporation method using Gene Plus II (Bio-Rad Laboratories, Hercules, California). Briefly, 3 μg of DsRed2-express plasmid was mixed with 2 million SHIN3 cells in 400 μL of the cell culture media (RPMI 1640 with 10% FCS). Then the cell suspension was put in a pulse cuvette

(Bio-Rad Laboratories) and 250-V pulses were delivered after 950 cycles.

2.4 Fluorescence Microscopy

SHIN3 cells (1×10^4) were plated on a cover glass bottom culture well and incubated for 16 h. BSA-RhodG, GmSA-RhodG, or Av-RhodG was added to the medium (5 nmol/L) and the cells were incubated for 1 or 3 h. Cells were washed one time with phosphate-buffered solution (PBS) and fluorescence microscopy was performed using an Olympus BX51 microscope (Olympus America Inc., Melville, New York) equipped with the following filters: excitation wavelength 470 to 490 nm and emission wavelength 515-nm long pass. Transmitted light differential interference contrast (DIC) images were also acquired.

2.5 Flow Cytometry

One-color flow cytometry was performed for the assessment of the fluorescing capability of Av-RhodG, GmSA-RhodG, and BSA-RhodG in SHIN3 cancer cells. SHIN3 cells (1×10^5) were plated on a 12-chamber culture well and incubated for 16 h. Av-RhodG, GmSA-RhodG, or BSA-RhodG was added to the medium (20 nmol/L) and the cells were incubated for 1, 3, and 6 h. For the assessment of competitive binding of GmSA-RhodG and avidin-RhodG, SHIN3 cancer cells were incubated with a large amount of excess GmSA (143 $\mu\text{mol}/\text{L}$) for 1 h. At 1 h after incubation with or without GmSA, Av-RhodG was added to a concentration of 300 nmol/L and incubated for an additional 3 h. Cells were washed once with PBS and trypsinized, and then flow cytometry was performed. A 488-nm argon ion laser was employed for excitation. Signals from cells were collected using a 530/30-nm band pass filter. Cells were analyzed in a FACScan cytometer (Becton Dickinson, Franklin Lakes, New Jersey), and all data were analyzed using CellQuest software (Becton Dickinson). The fluorescence intensity of each fluorophore was termed the mean fluorescence index (MFI). A regression line was calculated from the data sets of incubation time and common logarithmic value of MFI, and then plotted as a function of incubation time using Microsoft Excel 2003 (Microsoft, Redmond, Washington). The MFI value at each time point and the slope of the regression line were compared among the three fluorophores.

2.6 Measurement of Fluorescence Intensity of Fluorophore Conjugates *In Vitro*

To compare the fluorescing capability of Av-RhodG, GmSA-RhodG, and BSA-RhodG *in vitro*, fluorescence intensity and emission spectra of Av-RhodG, GmSA-RhodG, and BSA-RhodG were measured by the Maestro™ *In-Vivo* Imaging System (CRI Inc., Woburn, Massachusetts) in arbitrary units [(a.u.)]. Av-RhodG, GmSA-RhodG, and BSA-RhodG (50 pmol/400 μL PBS) were put in a nonfluorescent 96-well plate (Costar, Corning Incorporated, Corning, New York) and spectral fluorescence imaging was performed. A bandpass filter from 445 to 490 nm and a long pass filter over 515 nm were used for emission and excitation light, respectively. The tunable filter was automatically stepped in 10-nm increments from 500 to 800 nm while the camera captured images at each wavelength interval with constant exposure. Spectral un-

mixing algorithms were applied to create the unmixed image of the three probes. A region of interest (ROI) as large as each well was drawn to determine the emission spectra and the fluorescence intensity of three probes using commercial software (Maestro).

2.7 Animal Model of Peritoneal Metastases

All procedures were carried out in compliance with the *Guide for the Care and Use of Laboratory Animal Resources* (1996), National Research Council, and approved by the National Cancer Institute Animal Care and Use Committee. The intraperitoneal tumor xenografts were established by intraperitoneal injection of 2×10^6 SHIN3 or SHIN3 transfected with RFP DsRed2 cells suspended in 200 μL of PBS in female nude mice (National Cancer Institute Animal Production Facility, Frederick, Maryland). Experiments with tumor-bearing mice were performed at 14 days after injection of the cells.

2.8 In Vivo Spectral Fluorescence Imaging

500 pmol Av-RhodG, GmSA-RhodG, and BSA-RhodG were diluted in 300 μL PBS and injected into the peritoneal cavities of mice with peritoneally disseminated cancer implants. Each set of three mice (one for each fluorophore) was repeated in triplicate. Three hours after intraperitoneal injection, all three mice were sacrificed with carbon dioxide inhalation. Immediately after sacrifice, the abdominal cavity was exposed and the three mice were placed side by side on a nonfluorescent plate to compare the fluorescence intensity of the tumors. Spectral fluorescence images were obtained using Maestro. Whole abdominal images as well as closeup images of the peritoneal membrane were obtained. A bandpass filter from 445 to 490 nm and a long pass filter over 515 nm were used for emission and excitation light, respectively. The tunable filter was automatically stepped in 10-nm increments from 500 to 800 nm while the camera captured images at each wavelength interval with constant exposure. The spectral fluorescence images consisting of autofluorescence spectra and the spectra from the probes were obtained, and then, unmixed based on their spectral patterns using commercial software (Maestro).

Using the unmixed fluorescence image of the three peritoneal membranes, fluorescence intensity of the cancer implants was semiquantitatively compared among the three probes. A ROI as large as the peritoneal membrane was drawn inside the bowel, and a histogram (number of pixels at specific fluorescence intensity) was created using ImageJ software (<http://rsb.info.nih.gov/ij/plugins/mri-analysis.html>). Then, a threshold was set in the fluorescence intensity above which a pixel is counted. The total number of pixels (N) within the threshold range was calculated at a threshold value of t

$$N(t) = \sum_{i=t}^{\infty} n(i), \quad (1)$$

where i is the fluorescence intensity in arbitrary units, n is the number of pixels at the fluorescence intensity of i , t is the threshold value, and N is the total number of pixels within the threshold range ($i \geq t$). The common logarithm (\log) values of N were calculated and plotted as a function of t . The regression line was calculated from these data sets (t and $\log N$)

using Microsoft Excel 2003. For comparison of the fluorescent intensity or the "brightness," the slope of regression line was compared among the three fluorophores.

2.9 Assessment of the Sensitivity and Specificity of GmSA-RhodG for the Detection of Peritoneal Cancer Foci

The sensitivity and specificity of GmSA-RhodG imaging for the detection of peritoneal disseminated cancer foci were studied using three tumor-bearing mice. The intraperitoneal tumor xenografts were established 14 days after intraperitoneal injection of 2×10^6 RFP-transfected SHIN3 cancer cells suspended in 200 μL of PBS in female nude mice (National Cancer Institute Animal Production Facility). Three hours after intraperitoneal injection of 500 pmol GmSA-RhodG diluted in 300 μL PBS, spectral fluorescence images of the peritoneal membranes were obtained by Maestro. For each mouse, two different parts of the peritoneal membranes were randomly selected and spread out on a nonfluorescent plate and closeup spectral fluorescence imaging was performed. ROIs were drawn both within the nodules depicted by RFP spectral unmixed images (standard reference for cancer foci) and in the surrounding adjacent areas (standard reference for noncancerous foci), and the average fluorescence intensity of each ROI was calculated both on the RFP and the GmSA-RhodG spectral unmixed images using commercial software (Maestro version 2). The number of ROIs drawn in the noncancerous areas was the same as that drawn in the cancer foci. All visible nodules with short-axis diameters ≥ 1 mm and average fluorescence intensities ≥ 2 (a.u.) on RFP spectral unmixed images were included for analysis, because the minimum possible diameter for ROI drawing was 1 mm and the minimum visible fluorescence intensity was 2 (a.u.). Then, additional ROIs were drawn in the nodules depicted only by the spectral unmixed GmSA-RhodG images to count the number of false positive lesions. The average fluorescence intensities of false positive foci were calculated both on the RFP and the GmSA-RhodG unmixed images. Positivity for GmSA-RhodG was defined as average fluorescence intensity ≥ 10 (a.u.), whereas for a negative for GmSA-RhodG was defined as average fluorescence intensity < 10 (a.u.) on the spectral unmixed GmSA-RhodG images. The numbers of foci positive for both GmSA-RhodG and RFP, negative for both GmSA-RhodG and RFP, and positive only for GmSA-RhodG or RFP were counted. *Sensitivity* of GmSA-RhodG for the detection of peritoneal cancer foci was defined as the number of peritoneal foci positive for both GmSA-RhodG and RFP divided by number of peritoneal foci positive for RFP. *Specificity* of GmSA-RhodG was defined as the number of peritoneal foci negative for both RFP and GmSA-RhodG divided by number of peritoneal foci negative for RFP.

3 Results

3.1 Optical Characteristics of Av-RhodG, GmSA-RhodG, and BSA-RhodG

Prior to *in vivo* study, preinjection fluorescence intensities as well as the emission spectra of 50 pmol Av-RhodG, GmSA-RhodG, and BSA-RhodG in 400 μL PBS were assessed. The fluorescence intensities of Av-RhodG, GmSA-RhodG, and

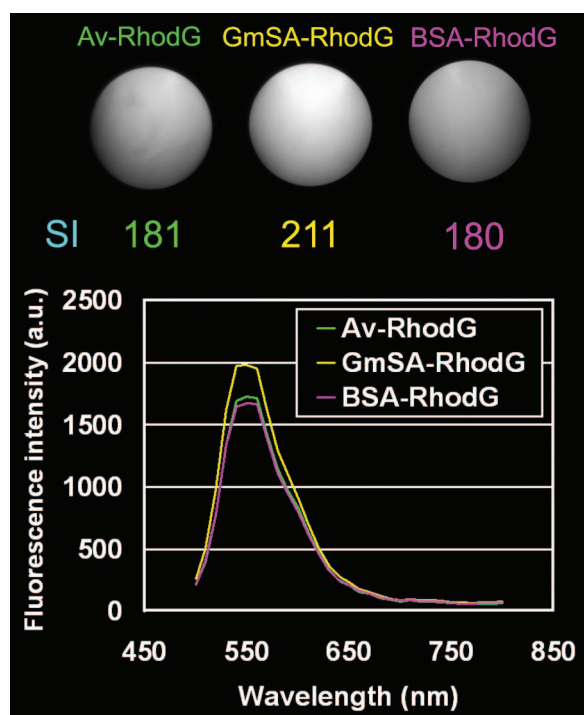


Fig. 1 Av-RhodG, GmSA-RhodG, and BSA-RhodG have the similar fluorescing capability and emission spectra. The fluorescence signal intensities (SI) of 50 pmol Av-RhodG, GmSA-RhodG, and BSA-RhodG in 400 μ L PBS were 181, 211, and 180 (a.u.), respectively. All 3 probes have the same emission peak at 550 nm when the tunable filter was stepped in 10-nm increments using the Maestro.

BSA-RhodG were 181, 211, and 180 (a.u.), respectively (Fig. 1). The emission spectra of these three probes were comparable with the same emission peak at 550 nm (Fig. 1). GmSA-RhodG showed the highest and BSA-RhodG showed the lowest fluorescence intensity. The difference of fluorescence intensity between BSA-RhodG and GmSA-RhodG was within 15% of GmSA-RhodG fluorescence intensity.

3.2 Flow Cytometry Analysis Demonstrates that GmSA-RhodG Cellular Uptake is Significantly Higher than Av-RhodG

At 1, 3, and 6 h after incubation with 20 nmol/L Av-RhodG, GmSA-RhodG, or BSA-RhodG, one-color flow cytometry was performed. GmSA-RhodG showed a significant rightward shift (>one order shift) as compared with SHIN3 control cells at 3 and 6 h after incubation, while BSA-RhodG showed a minimal shift at all time points [Fig. 2(a)]. The percent of positive cells (M1) in Av-RhodG, GmSA-RhodG, and BSA-RhodG were 9.3, 96.4, and 2.1% for 1 h; 15.3, 99.8, and 2.8% for 3 h, 39.4, 99.8, and 2.8% for 6 h, respectively. The rate of uptake, as shown by the slope of regression lines calculated from the data sets of incubation times and common logarithm values of the MFI, were 0.043, 0.147, and 0.004 (a.u./h) for Av-RhodG, GmSA-RhodG, and BSA-RhodG, respectively. The absolute MFI values at all time points and the increase rates of MFI uptake values were consistently higher for GmSA-RhodG than Av-RhodG, whereas BSA-RhodG showed little or no increase in MFI values. These results indicate that the GmSA-RhodG more effectively accumulates

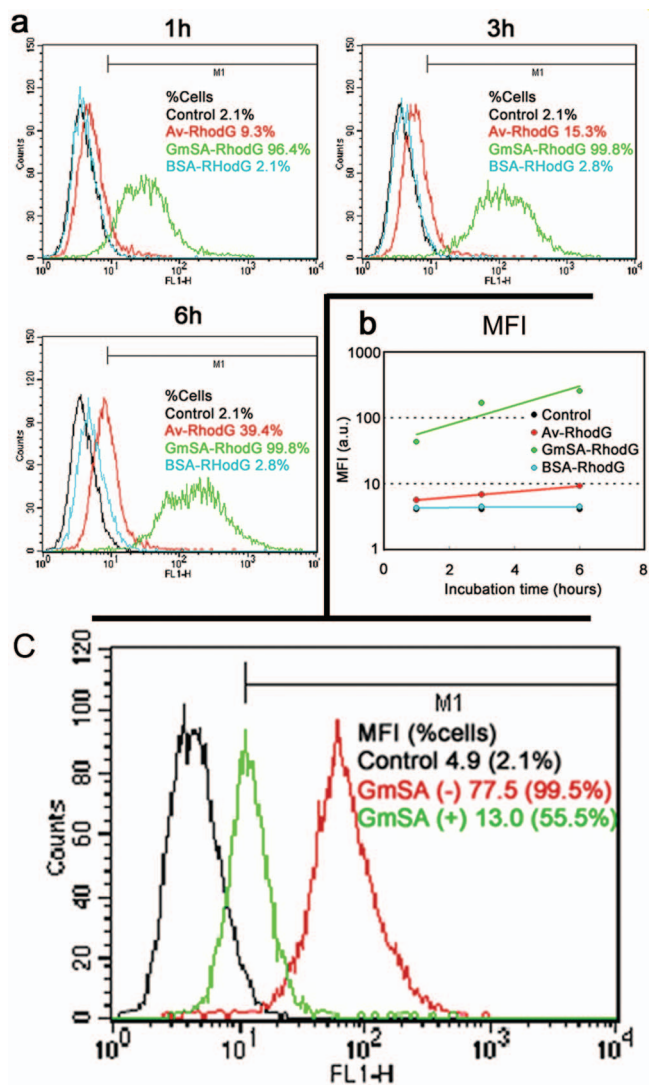


Fig. 2 Flow cytometry analysis shows that uptake of GmSA-RhodG is higher than that of Av-RhodG but GmSA-RhodG and Av-RhodG competitively bind to the same receptor. (a) Serial flow cytometry was performed 1, 3, and 6 h after incubation with 20 nmol/L Av-RhodG (red), GmSA-RhodG (green), and BSA-RhodG (blue) as well as unstained control (black). The percents of positive cells (M1) of Av-RhodG, GmSA-RhodG, and BSA-RhodG were 9.3, 96.4, and 2.1% at 1 h, 15.3, 99.8, and 2.8% at 3 h, 39.4, 99.8, and 2.8% at 6 h after incubation, respectively. The MFI values of GmSA-RhodG were higher and plot overlay of GmSA-RhodG demonstrated larger rightward shift than Av-RhodG or BSA-RhodG at any time point. The slopes of regression lines, calculated from the data sets of incubation time and common logarithm value of MFI, were 0.043, 0.147, and 0.004 [(a.u.)/h] for Av-RhodG, GmSA-RhodG, and BSA-RhodG, respectively. (b) Flow cytometry analysis of Av-RhodG accumulation into SHIN3 cancer cells with (green) or without (red) preincubation with high dose GmSA. Both MFI values and percents of positive cells (M1) were suppressed by 1-h preincubation with 143 μ mol/L GmSA. The percents of positive cells and the MFI values decreased from 99.5% and 77.5 (a.u.) to 55.5% and 13.0 (a.u.), respectively by GmSA administration.

within SHIN3 cancer cells and that the accumulation of GmSA-RhodG is mediated by galactosylation on albumin because the chemically similar BSA-RhodG had substantially reduced uptake.

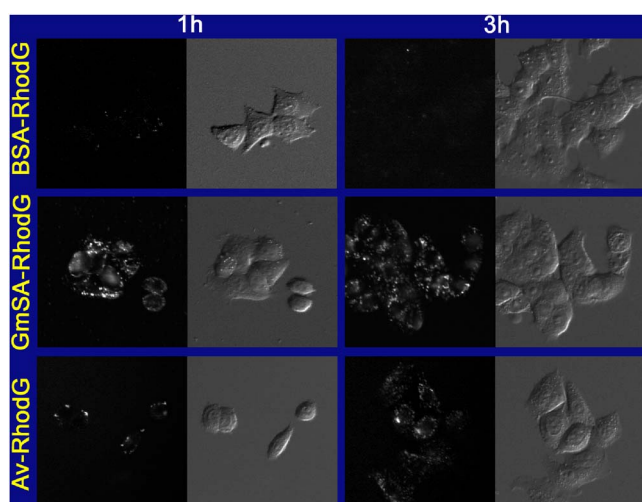


Fig. 3 Av-RhodG and GmSA-RhodG are internalized into the SHIN3 cancer cells but BSA-RhodG is not. Serial fluorescence microscopy (left panel) and differential interference contrast imaging (right panel) were performed 1 and 3 h after incubation with 5 nmol/L BSA-RhodG, GmSA-RhodG, or Av-RhodG. Fluorescence microscopy of SHIN3 cancer cells cultured with GmSA-RhodG and Av-RhodG demonstrated a large number of fluorescent dots within the cytoplasm as early as 1 h after incubation. The number of fluorescent dots within the cytoplasm increased 3 h after incubation with GmSA-RhodG and Av-RhodG. However, more fluorescent dots were seen in GmSA-RhodG than Av-RhodG under the same photographic exposure time and the same magnification. BSA-RhodG showed no fluorescent dots within the SHIN3 cancer cells. Original magnification: $\times 200$. Photographic exposure time: 1 s.

3.3 Competitive Inhibition of Binding between GmSA-RhodG and Av-RhodG

To assess whether Av-RhodG and GmSA-RhodG compete for the same receptor, the D-galactose (asialoglycoprotein) receptor on the SHIN3 cancer cell, the competitive inhibition of Av-RhodG binding and internalization was evaluated by adding a large amount of GmSA prior to incubation with Av-RhodG. Flow cytometry analysis demonstrated that in the absence of GmSA, the MFI of Av-RhodG in SHIN3 cancer cells increased from 4.9 to 77.5 (a.u.) during 3-h incubation, whereas, when GmSA was administered prior to Av-RhodG, the MFI only increased from 4.9 to 13.0 (a.u.) (83% reduction) [Fig. 2(b)]. The percent of positive cells was 99.5% for those without preincubation with GmSA, and the percentage of positive cells was 55.5% (44% reduction) for those with preincubation with GmSA. These results indicate that Av-RhodG and GmSA-RhodG compete for the same receptor of SHIN3 cancer cell.

3.4 Fluorescence Microscopy of Internalized GmSA-RhodG and Av-RhodG in SHIN3 Ovarian Cancer Cells

To study the cellular location of each probe, fluorescence microscopy and DIC imaging were performed 1 and 3 h after incubation with 5 nmol/L Av-RhodG, GmSA-RhodG, or BSA-RhodG. Fluorescence microscopy of SHIN3 cells cultured with GmSA-RhodG and Av-RhodG showed a large number of fluorescent dots within the cytoplasm as early as

1 h after incubation (Fig. 3). The number of fluorescent dots increased over 3-h incubation with GmSA-RhodG and Av-RhodG; however, the number of GmSA-RhodG dots was larger and more apparent than Av-RhodG dots both at 1 and 3 h after incubation. BSA-RhodG showed no fluorescent dots within the cells at any time. These results indicate that both GmSA-RhodG and Av-RhodG are internalized within SHIN3 cancer cells and are likely located within the endoplasmic vesicles or lysosomes,⁴ but GmSA-RhodG are more effectively internalized into the cells based on the number and size of internalized dots.

3.5 Comparison of In Vivo Spectral Fluorescence Imaging of Ovarian Cancer Implants with Av-RhodG, GmSA-RhodG, and BSA-RhodG

To compare the fluorescence intensities of the cancer implants *in vivo*, spectral fluorescence imaging was performed 3 h after an intraperitoneal injection of 500 pmol Av-RhodG, GmSA-RhodG, or BSA-RhodG. Three mice injected with each of the three probes were placed side by side on a non-fluorescent plate, and spectral fluorescence images of the abdominal cavities and closeup images of the peritoneal membranes were obtained. Both GmSA-RhodG and Av-RhodG clearly depicted the aggregated tumor foci as well as submillimeter implants *in vivo* (Fig. 4). However, BSA-RhodG failed to depict the tumor foci due to the insufficient fluorescence. The visual assessment of spectral fluorescence images revealed that the signal intensity from the cancer implants exposed to GmSA-RhodG was higher than that of Av-RhodG.

To objectively analyze the fluorescence intensities of the peritoneal implants among the three optical probes, a ROI encompassing the peritoneal membrane and circumscribed by the colon was drawn on the unmixed RhodG fluorescence image [Fig. 5(a)] and a histogram depicting the distribution of pixel intensities was created [Fig. 5(b)]. The dynamic range of signal intensity in the unmixed fluorescence image was set from 1 to 256 (a.u.) and the threshold value (t) was changed from 31 to 241 in increments of 10, because the background signals, such as the normal peritoneal membrane excluding tumors and the nonfluorescent plate, were mostly less than 31 (a.u.). Then, the total number of pixels (N) within the threshold range was calculated as a function of threshold (t), and a regression line was calculated in each ROI [Fig. 5(c)]. The slopes of Av-RhodG, GmSA-RhodG, and BSA-RhodG were -0.0362 , -0.0092 , and -0.1074 , respectively. These results indicate that the *in vivo* fluorescence of the GmSA-RhodG is higher than Av-RhodG, and the galactosylation of albumin is essential for binding ovarian cancer cells.

3.6 Sensitivity and Specificity of GmSA-RhodG In Vivo Spectral Fluorescence Imaging to Detect RFP-Transfected Peritoneal Cancer Foci

To investigate the effectiveness of GmSA-RhodG, sensitivity and specificity of spectral unmixed GmSA-RhodG imaging for peritoneal cancer foci was studied using dual color *in vivo* spectral fluorescence imaging of RFP DsRed2 and RhodG [Fig. 6(a)]. A total of 283 peritoneal cancer foci in 3 mice were identified by the spectral unmixed RFP images [Fig. 6(b)]. An additional 283 corresponding ROIs were created in the noncancerous areas. No foci showed GmSA-RhodG fluo-

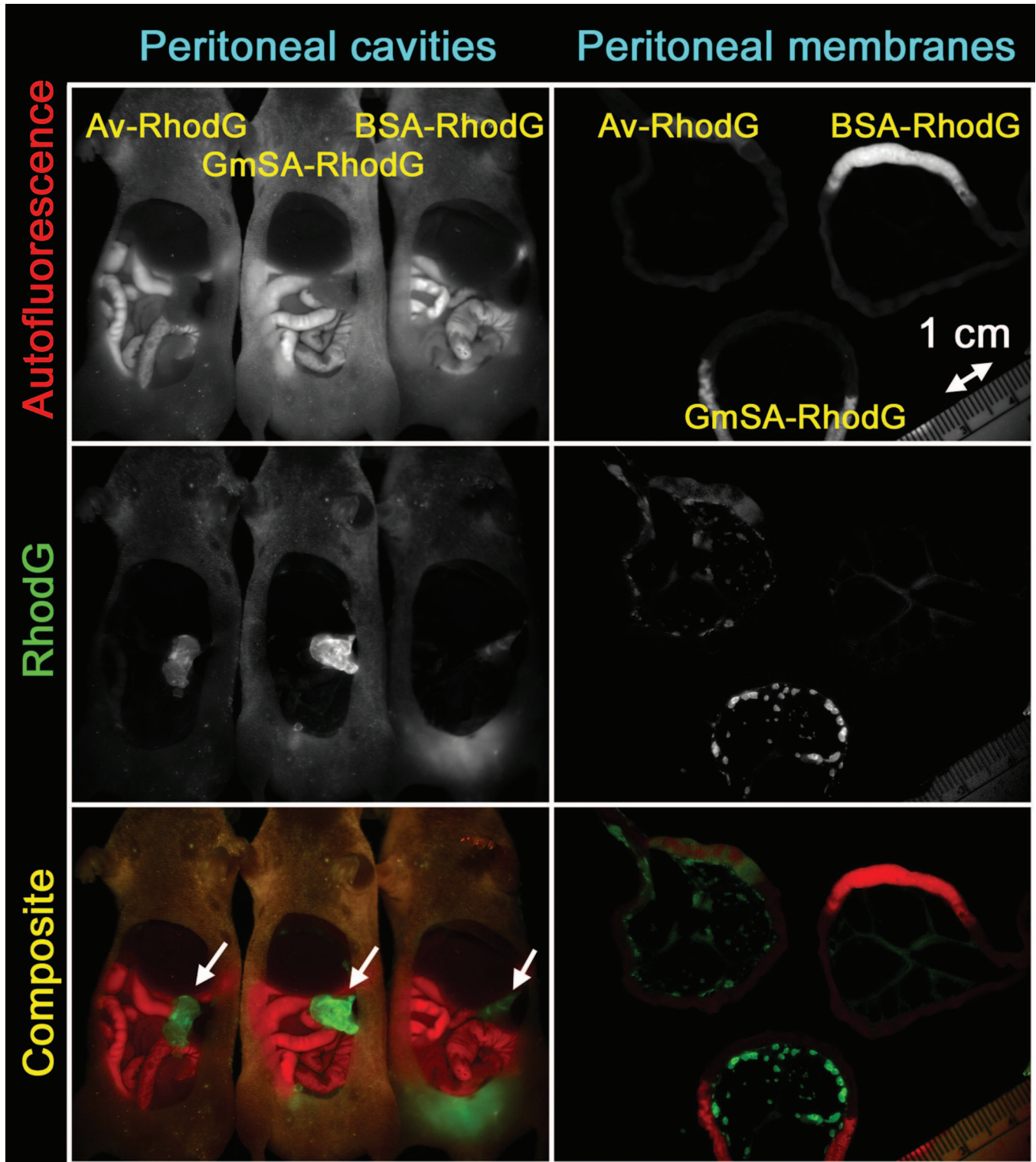


Fig. 4 GmSA-RhodG visualized the peritoneal cancer foci more clearly than Av-RhodG due to the higher signal intensity from the cancer foci. Spectral fluorescence imaging of the peritoneal cavities and the closeup peritoneal membranes of tumor-bearing mice were performed 3 h after intraperitoneal injection of 500 pmol Av-RhodG, GmSA-RhodG, and BSA-RhodG. Spectral unmixed autofluorescence (upper), RhodG fluorescence (middle), and composite (lower) images of three mice instilled with Av-RhodG, GmSA-RhodG, or BSA-RhodG are shown. Aggregated tumor foci (arrows) as well as the small cancer implants on the peritoneal membranes were detected by Av-RhodG and GmSA-RhodG. However, GmSA-RhodG visualized the cancer foci more clearly than Av-RhodG because of the higher signal intensities from the cancer foci. BSA-RhodG failed to depict the cancer foci due to the insufficient signal intensities from the cancer foci.

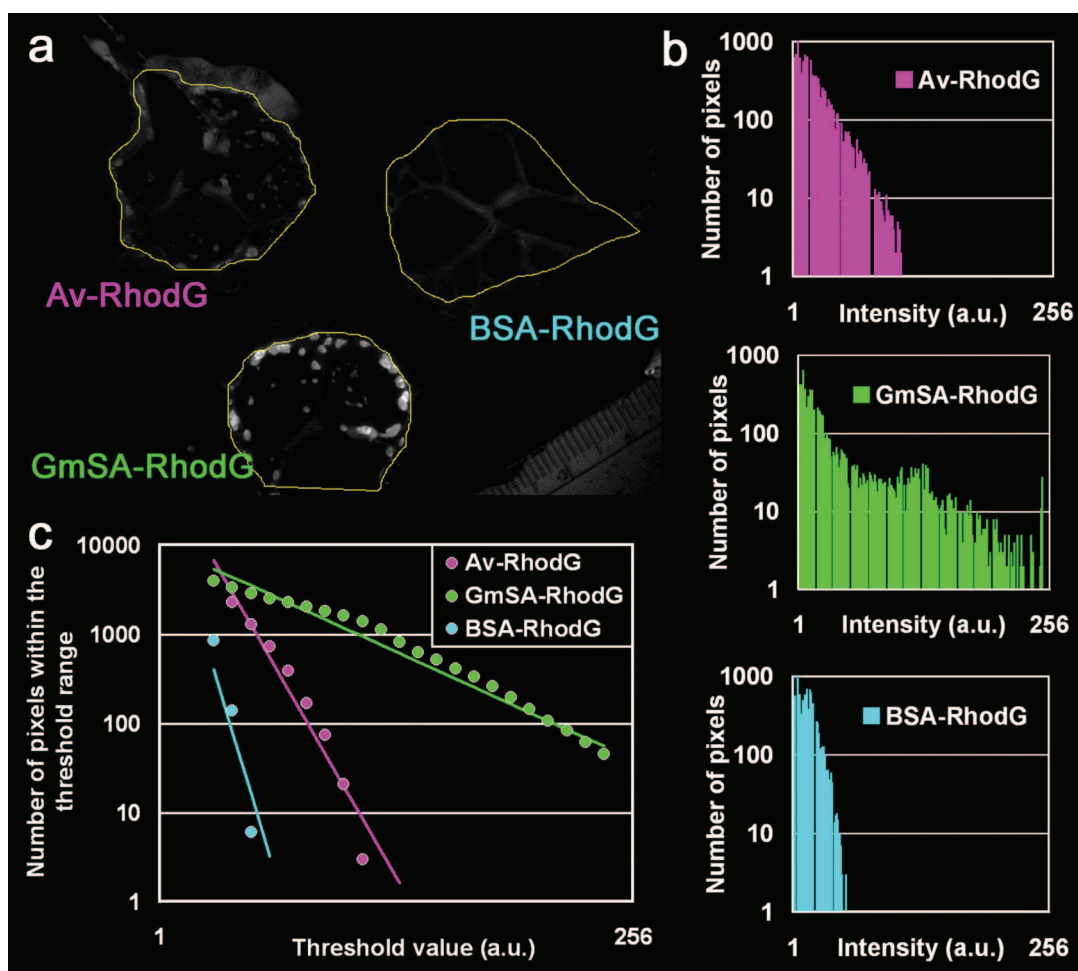


Fig. 5 GmSA-RhodG showed the higher fluorescence intensity on *in vivo* spectral fluorescence imaging than Av-RhodG. *In vivo* fluorescence intensity of the peritoneal cancer foci was semiquantitatively assessed using the spectral unmixed RhodG image. (a) ROI was drawn inside the intestine of each of the peritoneal membranes instilled with three optical probes, Av-RhodG, GmSA-RhodG, and BSA-RhodG (the same image as the unmixed green fluorescence image of Fig. 4). (b) Histogram of fluorescence intensity of a ROI drawn on each peritoneal membrane instilled with Av-RhodG, GmSA-RhodG, or BSA-RhodG. The dynamic range of the fluorescence intensity was split into 256 equal-sized bins (1 to 256). Then for each bin (horizontal axis), the number of pixels from the data set that fall into each bin (vertical axis) are counted. The shape of the plot distribution ≤ 30 (a.u.) is almost the same among the three histograms. (c) Regression lines of three probes. The regression lines were calculated from the data sets (fluorescence threshold values 31 to 241, total number of pixels within the threshold range 10 to 10 000 in common logarithm). The slopes of Av-RhodG, GmSA-RhodG, and BSA-RhodG were -0.0362 , -0.0092 , and -0.1074 , respectively. GmSA-RhodG has the highest slope value consistent with it being the brightest fluorophore; whereas, BSA-RhodG had the lowest slope value.

rescence intensities ≥ 10 (a.u.) among the 283 foci that were negative for RFP. However, another three foci were detected only by GmSA-RhodG images with no corresponding RFP focus (false positive foci). Thus, the spectral fluorescence imaging of GmSA-RhodG had a sensitivity of 100% (283/283) and a specificity of 99% (283/286).

4 Discussion

Prior reports have focused on the ability of avidin-fluorophore conjugates to target lectin binding proteins, also known as asialo receptors or β -D-galactose receptors, which are over-expressed on the cell surface of many cancers including ovarian cancer. Avidin is also readily absorbed through the peritoneal membrane, transported to the liver, and trapped by D-galactose receptors on hepatocytes,^{4,5,9} well away from the imaging field. In this manner, high target-to-background ratios

can be obtained in peritoneal implants. However, avidin is highly immunogenic and, therefore, not suitable as a clinical agent.

A galactosyl serum albumin (GSA), which is conjugated galactose molecules to the amino groups of albumin with a short spacer, has been reported to have affinity for the D-galactose receptors.¹⁰ This GSA has already been approved for human use when radiolabeled with technetium-99m (^{99m}Tc) using a diethylenetriamine pentaacetic acid and is commercially available in Japan and Europe as means of non-invasively assessing regional liver function by imaging the binding of ^{99m}Tc-labeled GSA to asialo receptors on hepatocytes.^{11,12} No immunological reaction against the GSA has been reported so far as expected. Similar to avidin, unbound GSA is absorbed rapidly through the peritoneum into circulation and then is quickly trapped by the asialo receptors

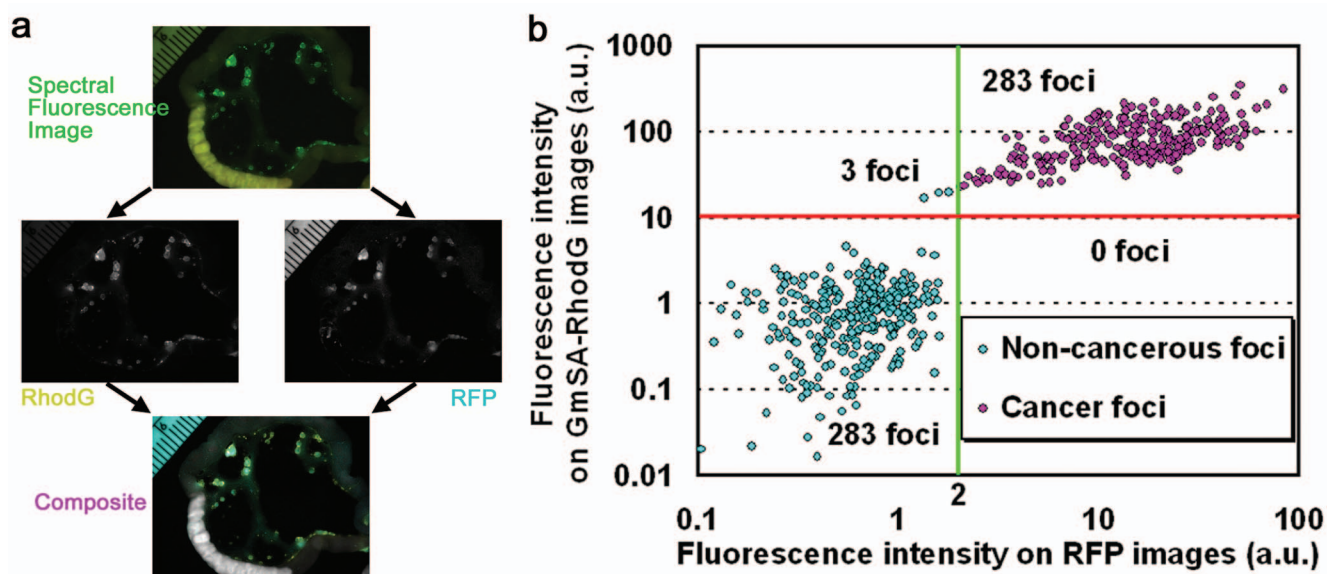


Fig. 6 Sensitivity and specificity of GmSA-RhodG spectral fluorescence imaging to detect peritoneal cancer foci are 100 and 99%, respectively. *In vivo* spectral fluorescence imaging of RFP-transfected SHIN3 ovarian cancer-bearing peritoneal membrane was performed 3 h after injection with 500 pmol GmSA-RhodG. (a) The spectral fluorescence image was unmixed based on the spectral patterns of RhodG and RFP as well as the autofluorescence, and then, a composite image consisting of RhodG (yellow), RFP (blue), and autofluorescence (black and white) was made. (b) Two-color *in vivo* fluorescence intensity plots of cancer foci and noncancerous foci. All visible foci with signal intensities ≥ 2 on spectral unmixed RFP images and diameters ≥ 1 mm were defined as cancer foci ($n=283$). For comparison, 283 ROIs were drawn in the surrounding peritumoral areas. Three foci were found only by the spectral unmixed GmSA-RhodG images. When foci positive for GmSA-RhodG were defined as those whose fluorescence intensities ≥ 10 , sensitivity and specificity of spectral unmixed GmSA-RhodG images to detect the presence of cancer foci were 100 and 99%, respectively.

on the hepatocytes of the liver, resulting in decreased background fluorescence in the peritoneal cavity.¹⁰ However, galactose conjugation to amino groups lowered the isoelectric point of GSA resulting in less accumulation in the peritoneal tumors than avidin.¹⁰ In this study, to enhance preferable chemical characteristics of avidin by multiplying binding sites and maintaining its high isoelectric point characteristics, conversion of serum albumin to GmSA involves galactosamine-conjugation using 23 D-galactosamines reacted with carboxyl groups rather than amino groups on an albumin molecule. Therefore, this GmSA is not only a viable clinical alternative to avidin but may also possess advantages over avidin as well as the conventional version of GSA.

The GmSA used in this study was composed of 1 molecule of BSA with 23 attached galactose molecules. The multivalency of binding sites on a binding reagent can enhance the binding affinity and minimize the binding off-rate.¹³ In contrast, avidin has only four sugar chains terminated with galactose molecules on the polypeptide chains of similar molecular weight to albumin. GmSA-RhodG showed enhanced accumulation within SHIN3 ovarian cancer cells compared with Av-RhodG, probably because of the multivalency of GmSA compared to avidin. It is theoretically possible that GmSA could be conjugated with up to 91 molecules of galactosamine and this could further increase the binding of GmSA to cancer cells.¹⁴

Compared to GmSA-RhodG, BSA-RhodG, which lacked galactosamine but was otherwise a similar chemical conjugate, showed minimal accumulation within SHIN3 cells. This is strong evidence that conjugation of galactosamine is re-

sponsible for the tumor specificity and that the binding mechanism involves interactions of conjugated galactosamine and the D-galactose receptor. We were able to confirm the sensitivity and specificity of GmSA-RhodG for ovarian cancer implants (for lesions at least 1 mm in size) using a RFP-transfected SHIN3 cell line. All lesions seen by RFP were also seen by GmSA-RhodG indicating a 100% sensitivity for lesions 1 mm or greater. Three foci identified by GmSA-RhodG were not confirmed by RFP and were considered false positives resulting in a 99% specificity. It is possible, that these lesions were, in fact, false negatives for RFP. For instance, using the spectral imaging method, both fluorophores were excited with a blue light (445 to 490 nm), so that RhodG was excited with better efficiency resulting in higher light output than RFP. In addition, the production of RFP is not uniform among the DsRed2-transfected SHIN3 cells (data not shown), probably because of the cell cycling and the speed of proliferation. Thus, the strength of the emission light from DsRed2-transfected SHIN3 tumors showed some variations at different locations even with similar sizes. Therefore, it is possible that GmSA-RhodG identified lesions that had undetectable emissions from RFP due to their small size. We attempted to equalize the emissions from the two fluorophores using two different excitation filters (445 to 490 nm for RhodG and 503 to 555 nm for RFP) to excite RhodG and RFP with similar efficiency without using the spectral technique; however, different inflection ratios of these two filters did not allow us to achieve perfect coregistration of the two images especially in tiny tumors. The clear distinction between GmSA-RhodG-

positive and GmSA-RhodG-negative foci as shown in Fig. 6 may indicate the high specificity of GmSA-RhodG. Although the high sensitivity and/or specificity can be determined for 1 mm or larger tumors, even smaller tumors are readily detectable with this method. Lesions as small as 100 μm were detectable but it is technically impossible with current image acquisition methods using Maestro to determine either the limits of size detection or the sensitivity and specificity for these nearly microscopic cancer clusters.

In view of the emphasis on near-infrared probes for *in vivo* imaging, it may be paradoxical that green fluorophores were used in this study. In general, green fluorophores (wavelengths 490 to 530 nm) are not ideal for *in vivo* imaging because of their short penetration within tissue. However, when the task is identifying surface lesions as is the case during surgery and endoscopy, green fluorophores are highly satisfactory.⁴ Green fluorophores not only provide sufficiently different spectra that they can usually be discriminated from background autofluorescence in the visible red spectrum but they generally have a high quantum yield resulting in very bright images compared to near-infrared probes, which are widely used for the *in vivo* fluorescence imaging from outside of the body.^{15,16}

5 Conclusion

Newly designed and synthesized GmSA-RhodG is able to identify tiny foci of peritoneal metastases due to ovarian cancer by binding to D-galactose receptors on the cell membrane. GmSA-RhodG is readily internalized within cancer cells and continues demonstrate high intensity fluorescence for at least 3 h after incubation with the agent. Using a RFP counterstain, GmSA-RhodG demonstrated a 100% sensitivity for peritoneal metastases 1 mm or greater in size and had a 99% specificity. This agent, which should not elicit immunogenic responses based on prior human experience of a similar reagent, may be suitable for clinical trials in women with ovarian cancer who are undergoing cytoreductive surgery.

Acknowledgments

This research was supported by the Intramural Research Program of the National Institutes of Health, National Cancer Institute, Center for Cancer Research and funded in part with federal funds from the National Cancer Institute, National Institutes of Health, under Contract No. N01-CO-12400.

References

1. P. R. Bargo, S. A. Prah, T. T. Goodell, R. A. Slevin, G. Koval, G. Blair, and S. L. Jacques, "In vivo determination of optical properties of normal and tumor tissue with white light reflectance and an em-

- pirical light transport model during endoscopy," *J. Biomed. Opt.* **10**(3), 034018 (2005).
2. X. Qi, M. V. Sivak, G. Isenberg, J. E. Willis, and A. M. Rollins, "Computer-aided diagnosis of dysplasia in Barrett's esophagus using endoscopic optical coherence tomography," *J. Biomed. Opt.* **11**(4), 044010 (2006).
3. M. A. Guicciardi, B. Andreoni, and E. Croce, "Mini-invasive surgery may be advised in oncology," *Crit. Rev. Oncol. Hematol.* **34**(3), 169–173 (2000).
4. Y. Hama, Y. Urano, Y. Koyama, M. Kamiya, M. Bernardo, R. S. Paik, M. C. Krishna, P. L. Choyke, and H. Kobayashi, "In vivo spectral fluorescence imaging of submillimeter peritoneal cancer implants using a lectin-targeted optical agent," *Neoplasia* **8**(7), 607–612 (2006).
5. Y. Hama, Y. Urano, Y. Koyama, P. L. Choyke, and H. Kobayashi, "Targeted optical imaging of cancer cells using lectin-binding BO-DIPY conjugated avidin," *Biochem. Biophys. Res. Commun.* **348**(3), 807–813 (2006).
6. G. Paganelli, M. Chinol, M. Maggiolo, A. Sidoli, A. Corti, S. Baroni, and A. G. Siccardi, "The three-step pretargeting approach reduces the human anti-mouse antibody response in patients submitted to radio-immunoscintigraphy and radioimmunotherapy," *Eur. J. Nucl. Med.* **24**(3), 350–351 (1997).
7. V. P. Hytonen, O. H. Laitinen, A. Grapputo, A. Kettunen, J. Savolainen, N. Kalkkinen, A. T. Marttila, H. R. Nordlund, T. K. Nyholm, G. Paganelli, and M. S. Kulomaa, "Characterization of poultry egg-white avidins and their potential as a tool in pretargeting cancer treatment," *Biochem. J.* **372**(Pt 1), 219–225 (2003).
8. S. Imai, Y. Kiyozuka, H. Maeda, T. Noda, and H. L. Hosick, "Establishment and characterization of a human ovarian serous cystadenocarcinoma cell line that produces the tumor markers CA-125 and tissue polypeptide antigen," *Oncology* **47**(2), 177–184 (1990).
9. H. Kobayashi, H. Sakahara, K. Endo, M. Hosono, Z. S. Yao, S. Toyama, and J. Konishi, "Comparison of the chase effects of avidin, streptavidin, neutravidin, and avidin-ferritin on a radiolabeled biotinylated anti-tumor monoclonal antibody," *Jpn. J. Cancer Res.* **86**(3), 310–314 (1995).
10. Z. Yao, M. Zhang, H. Sakahara, T. Saga, Y. Nakamoto, N. Sato, S. Zhao, Y. Arano, and J. Konishi, "Imaging of intraperitoneal tumors with technetium-99m GSA," *Ann. Nucl. Med.* **12**, 2, 115–118 (1998).
11. K. Sugahara, H. Togashi, K. Takahashi, Y. Onodera, M. Sanjo, K. Misawa, A. Suzuki, T. Adachi, J. Ito, K. Okumoto, E. Hattori, T. Takeda, H. Watanabe, K. Saito, T. Saito, Y. Sugai, and S. Kawata, "Separate analysis of asialoglycoprotein receptors in the right and left hepatic lobes using Tc-GSA SPECT," *Hepatology (Philadelphia, PA, U. S.)* **38**(6), 1401–1409 (2003).
12. Y. Hama, S. Kosuda, Y. Iwasaki, T. Kaji, and S. Kusano, "Technetium Tc 99m DTPA galactosyl human serum albumin to measure changes in hepatic functional reserve after transcatheter arterial embolization of the liver," *Can. Assoc. Radiol. J.* **52**(6), 399–403 (2001).
13. M. Tweedle, "Adventures in multivalency," *Contrast Media Mol. Imaging* **1**(1), 2–9 (2006).
14. A. H. Kwon, T. Inoue, and S. K. Ha-Kawa, "Characterization of the asialoglycoprotein receptor under hypoxic conditions in primary cultured rat hepatocytes," *J. Nucl. Med.* **46**(2), 321–325 (2005).
15. V. Ntziachristos, C. Bremer, and R. Weissleder, "Fluorescence imaging with near-infrared light: New technological advances that enable *in vivo* molecular imaging," *Eur. Radiol.* **13**(1), 195–208 (2003).
16. C. Bremer, V. Ntziachristos, and R. Weissleder, "Optical-based molecular imaging: Contrast agents and potential medical applications," *Eur. Radiol.* **13**(2), 231–243 (2003).